ACS OMEGA

http://pubs.acs.org/journal/acsodf

Article

Key Factors Governing the External Quantum Efficiency of Thermally Activated Delayed Fluorescence Organic Light-Emitting Devices: Evidence from Machine Learning

Haochen Shi, Wenzhu Jing, Wu Liu, Yaoyao Li, Zhaojun Li, Bo Qiao, Suling Zhao, Zheng Xu, and Dandan Song*

Cite This: *ACS Omega* 2022, 7, 7893−7900

Read Online

ACCESS | Metrics & More | Article Recommendations | Supporting Information

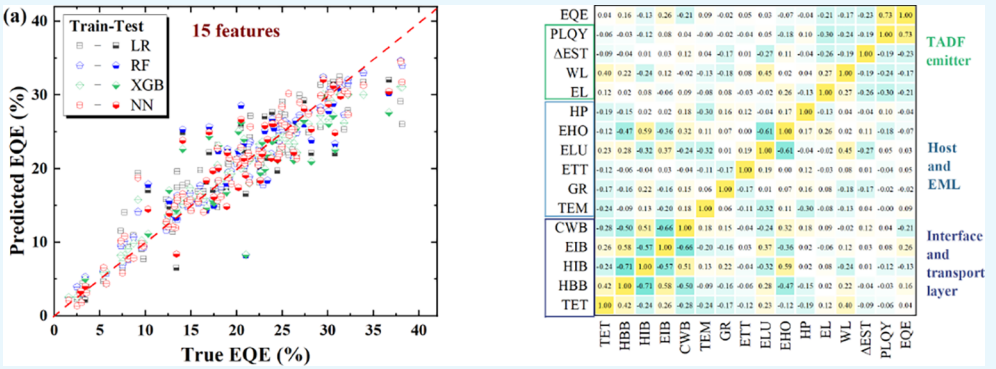

ABSTRACT: Thermally activated delayed fluorescence (TADF) materials enable organic light-emitting devices (OLEDs) to exhibit high external quantum efficiency (EQE), as they can fully utilize singlets and triplets. Despite the high theoretical limit in EQE of TADF OLEDs, the reported values of EQE in the literature vary a lot. Hence, it is critical to quantify the effects of the factors on device EQE based on data-driven approaches. Herein, we use machine learning (ML) algorithms to map the relationship between the material/device structural factors and the EQE. We established the dataset from a variety of experimental reports. Four algorithms are employed, among which the neural network performs best in predicting the EQE. The root-mean-square errors are 1.96 and 3.39% for the training and test sets. Based on the correlation and the feature importance studies, key factors governing the device EQE are screened out. These results provide essential guidance for material screening and experimental device optimization of TADF OLEDs.

INTRODUCTION

Thermally activated delayed fluorescence (TADF) materials have been regarded as the most promising third-generation emitters, which enable the fabrication of highly efficient organic light-emitting devices (OLEDs) due to their ability to utilize single triplets fully.[1,2] Compared to phosphorescent emitters with triplet exciton harvesting capability,[3] organic TADF emitters show great potential in reducing the cost for commercial applications as they require no noble metal in their molecular structures.[4] At present, TADF OLEDs possess high external quantum efficiencies (EQEs) with a theoretical limit beyond 20% and a practical record exceeding 38%.[5]

Despite the high level of the theoretical limit in EQE of TADF OLEDs, the reported values of EQE in the literature vary a lot, and many reports have EQEs much lower than 20%. It is generally considered that EQE is determined by the following expression:

$$\mathrm{EQE} = \eta_{\mathrm{OC}} \times \eta_{\mathrm{r}} \times \gamma \times \mathrm{PLQY}$$

where η_{OC} is the out-coupling efficiency, η_{r} is the ratio of the radiative excitons and highly depends on the reverse intersystem crossing (RISC) efficiency, γ represents the electron−hole balance, and PLQY is the photoluminescence quantum yield. Many factors affect these parameters, including the material and the device structural ones. For example, η_{OC} is determined by both the out-coupling technologies on the device and the dipole orientation of the TADF emitter.[6,7] Moreover, the factors affecting EQE may restrain each other. For instance, a host material enabling a low hole injection barrier (HIB) may induce a high electron injection barrier

Received: December 2, 2021
Accepted: February 14, 2022
Published: February 22, 2022

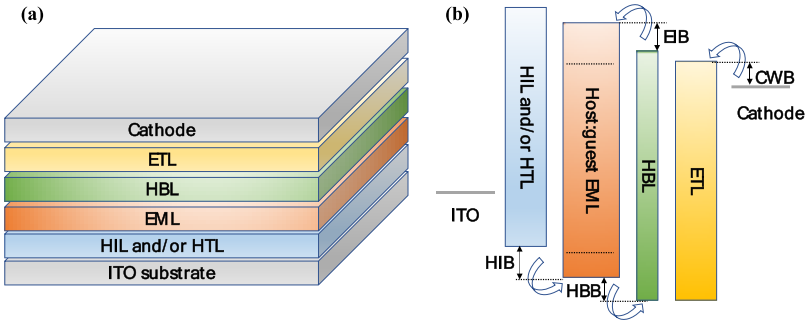

Figure 1. Schematic device structure (a) and energy level diagram (b) of TADF OLEDs.

Table 1. List of the Screened Material and Device Structural Factors[a]

abbreviation	full name	unit
EQE	external quantum efficiency	%
PLQY	photoluminescence quantum yield	%
WL	the electroluminescence peak wavelength of the TADF OLEDs	nm
EL	the prompt exciton lifetime of the TADF emitter	ns
ΔE_{ST}	the energy difference between the singlet and the triplet energy levels of the TADF emitter	eV
MW	the molar weight of the TADF emitter	g/mol
HP	the polarity of the host material	
HTg	the glass transition temperature (Tg) of the host	°C
EHO	the energy difference of the highest occupied molecular orbital (HOMO) energy level between the host and the TADF guest	eV
ELU	the energy difference of the lowest unoccupied molecular orbital (LUMO) energy level between the host and the TADF guest	eV
ETT	the classification of the energy difference of the triplet state between the host and the TADF guest, which is confined (the host has a larger triplet energy, or the band gap of the host is 1 eV or more larger than that of the guest) or nonconfined (others).	
GR	the doping ratio of the TADF guest in the emission layer (EML)	wt %
TEM	thickness of the EML	nm
TET	total thickness of the hole blocking layer (HBL) and the electron transport layer (ETL)/electron injection layer (EIL)	nm
CWB	the electron injection barrier from the cathode to the ETL/EIL	eV
EIB	the electron injection barrier, calculated using the energy difference between the LUMO values of the host and the HBL or the ETL/EIL	eV
HBB	the hole blocking barrier, calculated using the energy difference between the HOMO values of the host and the HBL or the ETL/EIL	eV
HIB	the hole injection barrier, calculated using the energy difference between the HOMO values of the HTL and the host	eV

[a]EQE is the output, while others are the input features.

(EIB), leading to modified electron−hole balance conditions in the emission layer (EML). As a result, to get a high EQE, it is rather complex for device design and material screening as there are so many material factors and device structural factors. Therefore, exploring the key factors governing the EQE and quantificationally mapping these factors with EQE are crucial to figuring out a whole picture for the approaches to making highly efficient TADF OLEDs.

Experimental evidence for the key factors is often reported but rarely quantified. Researchers need to do lots of trial and error experiments to quantify the relation between the factors and the EQE. Meanwhile, the real impact of the factors on EQE is challenging to assess in experimental studies, as the studies cannot adjust the factors solely and independently. Many parameters interplay with each other, which leads to deviations in evaluating the importance of a specific factor. For example, to assess the effect of PLQY on EQE, possible approaches involve altering the TADF emitters and/or the host materials and modifying the preparation parameters. These approaches may simultaneously change other factors like the molecular arrangement of the TADF emitters and/or the carrier mobility of the emission layer, leading to the changes in η_{OC} and η_r. Furthermore, an experimental investigation is challenging to give a quantified model to predict the device performance. Hence, it is critical to explore the mapping relation between the factors and the EQE of the TADF OLEDs based on data-driven approaches.

In the past decade, the machine learning (ML) approach has attracted increasing attention in the scientific field,[8−12] which can learn from the existing results and provide the relation between the input features to the output performance. Hence, it can establish the mapping relationship and make predictions with small errors. In this context, researchers in the material field use ML to quantify the properties (e.g., the electronic energy levels) of organic/inorganic materials with their structural features,[8−10] explore new materials for particular applications,[11,12] etc. In terms of devices, significant efforts are made on solar cells,[13−16] which provide some guidelines for material screening and device optimization of organic solar cells, perovskite solar cells, and CIGS solar cells. A prior study focuses on the blue phosphorescent OLEDs.[17] Though the learning performance still suffers from a large error, this study shows that ML can assist the device design of blue phosphorescent OLEDs. These preliminary demonstrations present the advantages of ML in exploring the correlations in the devices and providing guidelines for device optimization.

Hence, in this work, we attempt to use the ML approach to explore the quantificational relation between the EQE of TADF OLEDs and their material and device structural factors, aiming to screen out the key factors governing the EQE. To make the learning results more referable for experimental

https://doi.org/10.1021/acsomega.1c06820
ACS Omega 2022, 7, 7893−7900

optimization, we established the dataset from various experimental reports. It is evident that the most critical factors include PLQY, the emission wavelength, the ΔE_{ST} of the TADF emitter, and the dipole orientation descriptors, which shall be paid special attention in device optimization.

RESULTS AND DISCUSSION

The typical device architecture and the energy level diagram of TADF OLEDs are shown in Figure 1. We screened 17 factors, including material information of the TADF emitter, the properties of the host and the emission layer (EML), and the device structural factors (interfaces and transport layers), as listed in Table 1. The output performance is the maximum external quantum efficiency (EQE).

The dataset is based on experimental results. First, we searched for the recently published experimental results of the OLEDs with TADF materials as the emitter. To avoid the deviation that existed in film preparation, we only considered the devices fabricated by thermal evaporation. In addition, devices with out-coupling structures are excluded. Thus, we got approximately 300 data points (listed in Table S1) from the papers (the references are listed in Table S1). Second, we subtracted the values of the factors listed in Table 1 from information listed in Table S1. Here, to avoid inconsistency among different reports, the energy levels of the common materials were assigned to the same values for the same material other than the inconsistent values among various reports. For specific materials, the values reported in the corresponding references were used. The detailed values are also listed in Table S1. In addition, the glass transition temperature of the host (HTg) was referred to the literature.[7,18−20] The molecular weight (MW) of the TADF emitter was calculated from its molecular structure.

We first analyzed the data distribution of the factors and the EQE of the TADF OLEDs. Data summaries are listed in Table S2, and violin plots are shown in Figure S1. In general, the commonly obtained EQE and PLQY are in the range of 15−22% and 80−100%, respectively. They demonstrate the unique advantages of TADF materials used as emitters. However, it is surprising that the reports with EQE values less than 10% are so much despite the highest efficiency exceeding 38%. Other factors also show significant deviations, as can be seen from Figure S1. The significant deviations in these factors make manually exploring the key factors much confusing; hence, a data-driven, clear, and full view of the factors governing the EQE is critical.

Then, we use the correlation matrix to learn the linear correlation among the factors and the EQE. The results are depicted in Figure 2. Overall, to get a high EQE, a high PLQY is essential, showing a strong linear correlation with EQE. A small ΔE_{ST}, a short EL, a high HTg, a reasonably large HBB and EIB, and a small CWB and HIB lead to a high EQE, whereas other factors seem to have a negligible linear correlation with EQE.

To clearly show the relationship between the factors and the EQE, we plot the statistics of the EQE values changing with several factors, as shown in Figure 3 and Figure S2.

PLQY and Electroluminescence Wavelength (WL). From Figure 3a, it is clear that EQE roughly increases with increasing PLQY; hence, they show a strong positive correlation (the correlation coefficient is 0.73). Though EQE shows a small linear correlation coefficient of −0.17 with the emission peak wavelength (WL), it is notably influenced by the

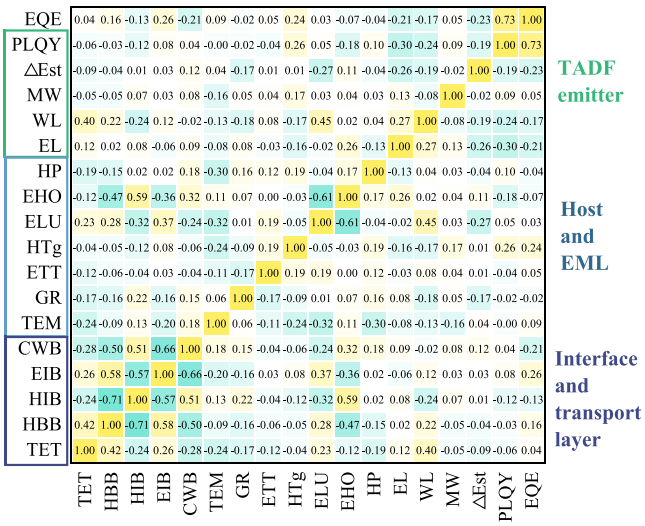

Figure 2. Correlation matrix of the material and device structural factors influencing the device EQE. The values represent the Pearson correlation coefficient (r). A high and positive value means a strong positive relation.

WL as shown in Figure 3b. In general, sky-blue to yellow devices in the wavelength scale of 480−550 nm exhibit a higher EQE, whereas blue (400−480 nm) and red (550−700 nm) devices suffer from a lower EQE. This trend is consistent with the general knowledge that blue and red devices have inferior performance to green devices. From experience, the inferior performance may correlate with the low PLQY of the TADF material. However, from Figure 3b, it can be seen that blue and red TADF emitters can achieve a high PLQY of approximately 100% as their green counterparts. Therefore, the inferior performances of the blue and red devices are probably induced by other factors in the devices.

ΔE_{ST} and Exciton Lifetime of the TADF Emitters. In TADF OLEDs, since EQE strongly depends on the reverse intersystem crossing (RISC) efficiency of the TADF emitters, a small ΔE_{ST} is required to facilitate the efficient RISC process;[21] the RISC rate constant (k_{RISC}) can be expressed by the Boltzmann distribution relation $k_{RISC} \propto e^{\Delta E_{ST}/k_B T}$, where k_B is the Boltzmann constant and T is the temperature. From Figure 3c, it is clear that most of the TADF emitters have a ΔE_{ST} of 0−0.2 eV, and the high EQE (≥30%) is obtained on a scale less than 0.1 eV. In general, EQE tends to decrease with increasing ΔE_{ST}. On the other hand, nonradiative recombination processes need to be suppressed to get a high EQE. These processes are governed significantly by the TADF emitters' exciton lifetime, and a short radiative lifetime tends to suppress nonradiative processes. TADF emitters generally have prompt lifetimes of 0−35 ns, which are much longer than those of the phosphorescent emitters (several to tens of microseconds).

Correlation between the Host and the TADF Guest: The Doping Ratio (GR) and the Energy Difference (EHO, ELU, and ETT). Doping TADF emitters into a host is an efficient way to get a high EQE benefiting from the suitable electrical property of the host and the suppressed recombination among the emitters. The doping ratio typically has an optimized value for the specific host−guest system and device structure. From Figure 3d, it shows that the guest ratio differs in an extensive range, while a relatively low ratio (around 10%) tends to enable both a high (≥30%) and low (≤10%) EQE.

https://doi.org/10.1021/acsomega.1c06820
ACS Omega 2022, 7, 7893−7900

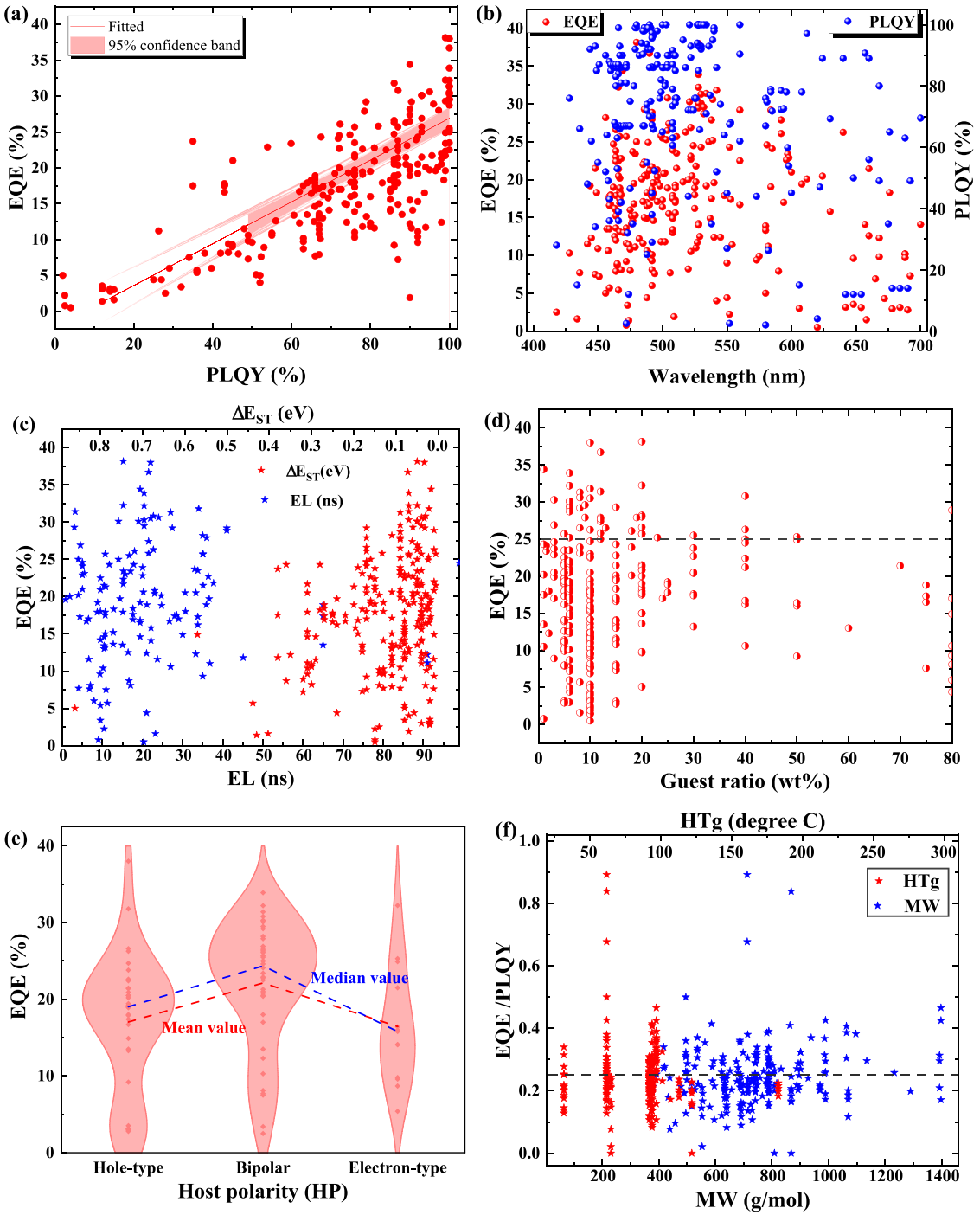

Figure 3. (a–f) Effects of different factors on EQE, (a) PLQY, (b) electroluminescence wavelength (WL), (c) ΔE_{ST} and prompt exciton lifetime (EL), (d) guest doping ratio (GR), and (e) host polarity (HP). (f) Effects of the dipole orientation descriptors (MW and HTg) on the EQE/PLQY ratio.

Therefore, the linear correlation coefficient between EQE and the GR is much tiny (−0.02). Essential requirements for the host generally include two aspects: (1) the host shall have a larger triplet energy than the TADF guest, and (2) the host is better to be bipolar to make the carrier distribution much balanced in the EML. Indeed, bipolar hosts tend to enable a higher EQE with a high mean value, while the electron-type host performs inferiorly. However, the effects of the energy differences between the host and the guest (EHO, ELU, and ETT) on EQE are indefinable from their correlations shown in Figure S2a.

Energy Barriers for Electrons and Holes (HIB, EIB, HBB, and CWB). The energy barriers for electrons and holes are also considered to be important in determining the device efficiency and the turn-on voltage. Reasonable values for energy barriers are expected to promote the carrier balance in the EML, which are generally considered factors in material screening. Therefore, they show strong correlations with each other. In terms of their effects on EQE, a larger EIB/HBB and a smaller CWB/HIB favor a high EQE. From the statistics of these barriers versus EQE (Figure S2b), a small HBB (<0 eV) and a large CWB/HIB (>0.75 eV) tend to lower the EQE,

https://doi.org/10.1021/acsomega.1c06820
ACS Omega 2022, 7, 7893−7900

whereas a large EIB has no such harmful effect. As most of the host materials are prone to transport holes, electrons are more difficult to be transported to the HTL/EML interface, while holes are facilely transported to the EML/HBL (or ETL) interface. A larger HBB can block holes at the EML/HBL (or ETL) interface, and a small CWB favors electron injection from the cathode to the ETL; hence, they lead to a high EQE. Though a larger EIB induces more difficulty in electron injection from the ETL/HBL, the electron injection to the guest is still facile as the guest typically has a lower LUMO than the host. Subsequent exciton formation directly on the guest between the injected electrons and the transported holes in the EML can also lead to a high EQE. In contrast, direct hole injection to the guest at the HTL/EML interface due to a large HIB leads to a low EQE.

Out-Coupling-Correlated Factors (MW of the TADF Emitter and HTg). In OLEDs, the horizontal orientation of the emissive transition dipole moment can improve the light out-coupling efficiency by up to 50% relative to a random orientation. Based on the analysis of 203 published emitter systems, Gather et al.[7] concluded that in host−guest systems with low-MW emitters, the orientation is mainly influenced by the host Tg, whereas the length and MW of the emitter become more relevant for systems involving higher-MW emitters. Figure 3f shows the effects of two crucial dipole orientation descriptors, MW of the guest and the host Tg (HTg), on the EQE/PLQY ratio ($= \eta_{OC} \times \eta_r \times \gamma$). Indeed, a large MW tends to get a high EQE/PLQY ratio by favoring high η_{OC}, whereas HTg has no definable effect on this ratio. This may be induced by the differences of the host materials in other aspects (like the energy levels) affecting this ratio through the charge balance (γ).

From the above analysis, it can be seen that these material and device structural features play complex influences on EQE, whose correlations are hard to be explored based on manually qualitative analysis. Hence, ML is required to process such complex correlations.

To quantitatively illustrate the factors governing the device performance, we use ML algorithms to map these factors to EQE. To establish the dataset for this learning, we remove the rows with missing data listed in Table S1. We employ four algorithms, including the linear regression (LR), neural network (NN), random forest (RF), and extreme gradient boosting (XGBoost). The input 15 features for the ML algorithms are listed in Table 1, excluding MW and HTg. MW and HTg effects will be discussed later. The dataset was randomly divided into 7:3 for training (the training set) and testing (the test set). The performance of the algorithm is evaluated by the root-mean-square error (RMSE) and Pearson's coefficient (r). The RMSE estimates the error between the predicted and true (experimental) values, and Pearson's coefficient (r) shows their linear correlation. Hence, an algorithm performs better with a lower RMSE and a higher r in prediction.

Table 2 lists the RMSE and r values on predicting the EQE values by various algorithms. Figure 4 plots the distributions of the true EQE and the predicted values by various algorithms. From the comparison of the true and predicted values shown in Figure 4a, it can be seen that the predicted values show fewer departures from the true values for NN, RF, and XGBoost models compared with the simple LR model. Among them, the NN performs best with the lowest RMSE (3.61%) on predicting the EQE of the test set.

Table 2. Performance of Different ML Algorithms on Predicting the EQE of the TADF OLEDs

		training set		test set	
input features	ML algorithms	RMSE (%)	r value	RMSE (%)	r value
15 features[a]	LR	3.44	0.86	3.94	0.71
	RF	1.53	0.97	4.69	0.60
	NN	2.28	0.92	3.61	0.55
	XGBoost	2.07	0.95	4.57	0.62
12 features[b]	LR	4.00	0.80	4.73	0.68
	RF	1.80	0.96	4.47	0.72
	NN	2.59	0.91	3.46	0.87
	XGBoost	1.27	0.98	3.91	0.78
14 features[c]	LR	3.13	0.87	4.52	0.65
	RF	1.56	0.97	3.81	0.75
	NN	1.96	0.95	3.39	0.81
	XGBoost	1.33	0.98	3.94	0.74

[a]Excluding HTg and MW listed in Table 1. [b]Excluding HTg, MW, HP, TEM, and ETT in Table S1. [c]Excluding HP, TEM, and ETT in Table S1.

To further screen the features, the importance of 15 input features is evaluated by the XGBoost model (shown in Figure 4b and listed in Table 3). As expected, PLQY is the most important feature governing the EQE. The emission peak wavelength (WL) is the second important factor, which reveals our analysis on the data statistics shown in Figure 3b. The prompt exciton lifetime (EL) and ΔE_{ST} also play notable roles in determining EQE as expected. It is a surprise that the guest doping ratio (GR) is so vital in determining EQE, as it shows negligible linear correlations with both EQE and PLQY (shown in Figure 2). This may be because the optimized doping ratio in many references is around 10% as shown in Figure 3d, while either a higher or lower doping ratio causes a lower EQE due to the enhanced exciton annihilation or the inefficient utilization of injected carriers, respectively. The three most minor important features are the HP, TEM, and ETT, showing negligible correlations with EQE and PLQY (Figure 2). Though the bipolar host seems to favor a high EQE demonstrated in the statistical analysis, it is not so crucial in the quantitative model established by XGBoost. The thickness of the EML (TEM) is an essential factor in device design and is always preoptimized, so it has little effect on EQE among different reports. A similar condition also occurs on ETT.

Considering that two factors may influence EQE simultaneously, we plot the statistics of the EQE values changing with two major factors, PLQY−ΔE_{ST} and PLQY−WL, as shown in Figure S3. A PLQY larger than 70% and a ΔE_{ST} less than 0.3 eV lead to a high EQE (>24%); meanwhile, a PLQY larger than 65% and a WL on the scale of 450−600 nm lead to a high EQE(>24%). This reveals that the major factors influence EQE simultaneously, which shall be considered in the experimental design.

Based on the analysis, we minimize the feature size to be 12, excluding three features: the HP, TEM, and ETT. The performances of the algorithms on the dataset with these 12 features are shown in Figure 5a and Table 2. It can be seen that the performances of all algorithms are better than or similar to those on the dataset with 15 features (shown in Figure 4a and Table 2). This indicates that the three features, the HP, TEM, and ETT, are nonsignificant factors on device EQE. The NN also performs best with the lowest RMSE and the highest r.

https://doi.org/10.1021/acsomega.1c06820
ACS Omega 2022, 7, 7893−7900

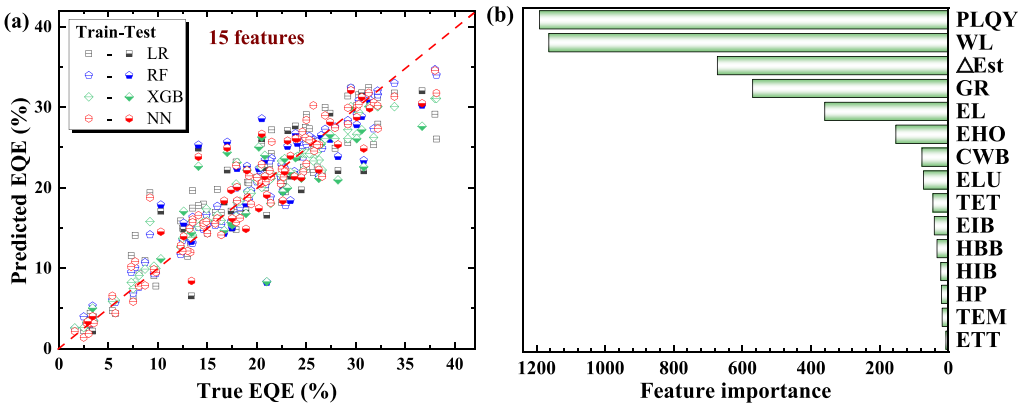

Figure 4. (a) Comparison of true EQE and predicted values by different algorithms on training and test sets with 15 input features listed in Table S1. XGB represents XGBoost. The red dashed line presents the condition in which the predicted value equals to the experimental value. (b) Feature importance of these 15 material and device structural features on EQE.

Table 3. The Three Most Important Factors Governing the EQE of the TADF OLEDs Evaluated by the XGBoost Model Based on Different Feature Sets

feature sets	first important	second important	third important
15 features	PLQY	WL	ΔE_{ST}
12 features	PLQY	WL	ΔE_{ST}
14 features	MW	WL	PLQY

The improvement in the prediction performance of the NN model can be ascribed to the decreased feature size, which minimizes the noise. The RF and XGBoost show minor improvements after feature minimization, as the excluded features are not important in these two models. The XGBoost and RF generally predict well except for several outliers.

These results confirm that the data-driven approach to predict the device performance is sufficiently referable for the experimental design of TADF OLEDs. Though the device performance can be well predicted in general, the device with an ultrahigh EQE (≥25%) shows a larger derivation between the predicted and the true values (shown in Figures 4a and 5b). One reason for this is that most of the data points have moderate performance, so the algorithms learn better due to the relatively larger data size and thus present a higher accuracy in the devices with good performance. In addition, several outliers can be observed in Figures 4a and 5a. These outliers are caused by other factors like the out-coupling effect, which are not considered in these models. For example, the outlier with a true EQE of 21% and a predicted value of less than 10% is probably caused by enhanced out-coupling efficiency despite of the low PLQY (45.1%) of the TADF emitter.[22] Hence, we further introduce the dipole orientation descriptors, MW and HTg, and the performance of algorithms is shown in Figure 5b and Table 2. The deviations of the outliers are decreased, proving that the dipole orientation indeed has a notable effect on EQE. Though the dipole orientation descriptors are not essential factors considered in material screening and device design, it shall be noted that they are very important and shall be considered.

As PLQY is of critical importance in determining EQE, we also tried to explore the key factors governing the PLQY from the viewpoints of the chemical structure and the chemical/physical properties of TADF molecules. We utilized the features including the MACCS fingerprint, E-state index, cheminformatics, ΔE_{ST}, the exciton lifetime, etc. and several algorithms (principal component analysis, LR, NN, RF, XGBoost, etc.) to analyze the correlations between these features of the TADF materials with PLQY. However, due to

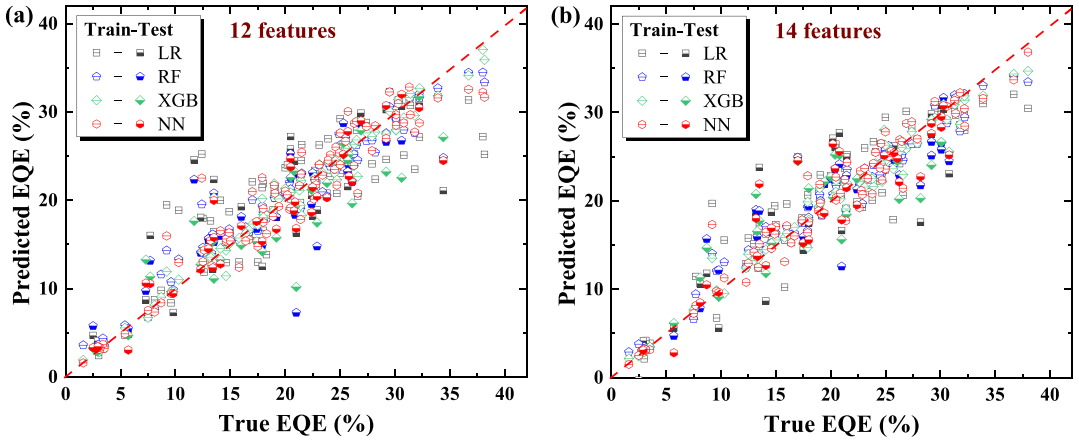

Figure 5. Comparison of true EQE and predicted values by different algorithms on training and test sets with 12 (a) and 14 (b) input features listed in Table S1. In the scenario of 12 features, HP, TEM, ETT, MW, and HTg are excluded, and the others listed in Table S1 are included. In the scenario of 14 features, MW and HTg are included. XGB represents XGBoost. The red dashed line presents the condition in which the predicted value equals to the experimental value.

https://doi.org/10.1021/acsomega.1c06820
ACS Omega 2022, 7, 7893−7900

the complexity of the molecules and the limited data size, the prediction accuracy is poor on the test set. Hence, guiding material design is still tricky by machine learning from the experimental results. Compared with the complexity of the molecules, the device structure is relatively simple, and the key features are limited; herein, the prediction on the device performance is much more accurate, which provides essential guidelines for device design and material screening.

CONCLUSIONS

In summary, key factors governing the device EQE of TADF OLEDs were explored and modeled by machine learning (ML) algorithms. These factors cover the properties of TADF emitters, the host and the EML, the transport layers, and the interfaces. Among the four used algorithms, the neural network performs best in predicting the EQE of the TADF OLEDs with a high accuracy. Key factors governing the device EQE are screened out based on correlation analysis and feature importance. To further improve the prediction accuracy, the optimizations of both the dataset and feature selection are important. These results prove the great potential and the power of the machine learning tool in optimizing the device EQE of TADF OLEDs, and the approach can also be applied in other types of OLEDs.

METHODS

Python (version 3.7) was employed as the platform for machine learning. Linear regression (LR), neural network (NN), random forest (RF), and extreme gradient boosting (XGBoost) algorithms were used for learning based on sklearn-linear_model, keras, sklearn-ensemble, and xgboost functions, respectively. The NN model had three hidden layers, which had 600, 600, and 600 neurons, respectively. The value of n_estimators in the RF model was 1000. The max depth and the objective in the xgboost function were 5 and "reg:gamma", respectively, and the value of n_estimators was 500. These values were optimized in advance. The ratio of the test set was 0.3. The algorithms were evaluated by the RMSE and r^2 value. Here,

$$\mathrm{RMSE} = \sqrt{\sum_{i=1}^{n} \frac{(X_i - Y_i)^2}{n}}$$

$$r^2 = 1 - \frac{\sum_{i=1}^{n} (X_i - Y_i)^2}{\sum_{i=1}^{n} (X_i - \overline{X})^2}$$

X_i, Y_i, $\overline{X}$, $\overline{Y}$, and n represent the i^{th} value of the experimental dataset, the i^{th} value of the predicted dataset, the mean value of the experimental dataset, the mean value of the predicted dataset, and the number of the dataset points, respectively.

ASSOCIATED CONTENT

Supporting Information

The Supporting Information is available free of charge at https://pubs.acs.org/doi/10.1021/acsomega.1c06820.

Detailed information of the input features and the external quantum efficiency of TADF OLEDs used in this work (Table S1), summary of screened factors and the EQE of the TADF OLEDs (Table S2), data distribution of screened factors and the EQE of the TADF OLEDs (Figure S1), effects of different factors on EQE (Figure S2), and relationship of EQE with PLQY−ΔE_{ST} and relationship of EQE with PLQY and the electroluminescence peak wavelength (WL) of the TADF OLEDs (Figure S3) (PDF)

AUTHOR INFORMATION

Corresponding Author

Dandan Song − *Key Laboratory of Luminescence and Optical Information, Beijing Jiaotong University, Ministry of Education, Beijing 100044, China; Institute of Optoelectronics Technology, Beijing Jiaotong University, Beijing 100044, China;* orcid.org/0000-0002-5050-8211; Phone: +86 13811566760; Email: ddsong@bjtu.edu.cn

Authors

Haochen Shi − *Key Laboratory of Luminescence and Optical Information, Beijing Jiaotong University, Ministry of Education, Beijing 100044, China; Institute of Optoelectronics Technology, Beijing Jiaotong University, Beijing 100044, China*

Wenzhu Jing − *Key Laboratory of Luminescence and Optical Information, Beijing Jiaotong University, Ministry of Education, Beijing 100044, China; Institute of Optoelectronics Technology, Beijing Jiaotong University, Beijing 100044, China*

Wu Liu − *Key Laboratory of Luminescence and Optical Information, Beijing Jiaotong University, Ministry of Education, Beijing 100044, China; Institute of Optoelectronics Technology, Beijing Jiaotong University, Beijing 100044, China*

Yaoyao Li − *Key Laboratory of Luminescence and Optical Information, Beijing Jiaotong University, Ministry of Education, Beijing 100044, China; Institute of Optoelectronics Technology, Beijing Jiaotong University, Beijing 100044, China*

Zhaojun Li − *Key Laboratory of Luminescence and Optical Information, Beijing Jiaotong University, Ministry of Education, Beijing 100044, China; Institute of Optoelectronics Technology, Beijing Jiaotong University, Beijing 100044, China*

Bo Qiao − *Key Laboratory of Luminescence and Optical Information, Beijing Jiaotong University, Ministry of Education, Beijing 100044, China; Institute of Optoelectronics Technology, Beijing Jiaotong University, Beijing 100044, China;* orcid.org/0000-0002-4416-7764

Suling Zhao − *Key Laboratory of Luminescence and Optical Information, Beijing Jiaotong University, Ministry of Education, Beijing 100044, China; Institute of Optoelectronics Technology, Beijing Jiaotong University, Beijing 100044, China;* orcid.org/0000-0003-0310-5628

Zheng Xu − *Key Laboratory of Luminescence and Optical Information, Beijing Jiaotong University, Ministry of Education, Beijing 100044, China; Institute of Optoelectronics Technology, Beijing Jiaotong University, Beijing 100044, China;* orcid.org/0000-0001-9680-2208

Complete contact information is available at: https://pubs.acs.org/10.1021/acsomega.1c06820

Notes

The authors declare no competing financial interest.

https://doi.org/10.1021/acsomega.1c06820
ACS Omega 2022, 7, 7893−7900

■ ACKNOWLEDGMENTS

This work was supported by the National Natural Science Foundation of China under Grant Nos. 61775013 and 62075006 and the Beijing Natural Science Foundation under Grant No. 2192045.

■ REFERENCES

(1) Endo, A.; Ogasawara, M.; Takahashi, A.; Yokoyama, D.; Kato, Y.; Adachi, C. Thermally activated delayed fluorescence from Sn(4+)-porphyrin complexes and their application to organic light emitting diodes–a novel mechanism for electroluminescence. *Adv. Mater.* **2009**, *21*, 4802−4806.
(2) Uoyama, H.; Goushi, K.; Shizu, K.; Nomura, H.; Adachi, C. Highly efficient organic light-emitting diodes from delayed fluorescence. *Nature* **2012**, *492*, 234−238.
(3) Baldo, M. A.; O'Brien, D. F.; You, Y.; Shoustikov, A.; Sibley, S.; Thompson, M. E.; Forest, S. R. Highly efficient phosphorescent emission from organic electroluminescent devices. *Nature* **1998**, *395*, 151−154.
(4) Zou, Y.; Gong, S.; Xie, G.; Yang, C. Design Strategy for Solution-Processable Thermally Activated Delayed Fluorescence Emitters and Their Applications in Organic Light-Emitting Diodes. *Adv. Opt. Mater.* **2018**, *6*, 1800568.
(5) Ahn, D. H.; Kim, S. W.; Lee, H.; Ko, I. J.; Karthik, D.; Lee, J. Y.; Kwon, J. H. Highly efficient blue thermally activated delayed fluorescence emitters based on symmetrical and rigid oxygen-bridged boron acceptors. *Nat. Photonics* **2019**, *13*, 540.
(6) Song, J.; Kim, K. H.; Kim, E.; Moon, C. K.; Kim, Y. H.; Kim, J. J.; Yoo, S. Lensfree OLEDs with over 50% external quantum efficiency via external scattering and horizontally oriented emitters. *Nat. Photonics* **2018**, *9*, 3207.
(7) Tenopala-Carmona, F.; Lee, O. S.; Crovini, E.; Neferu, A. M.; Murawski, C.; Olivier, Y.; Zysman-Colman, E.; Gather, M. C. Identification of the Key Parameters for Horizontal Transition Dipole Orientation in Fluorescent and TADF Organic Light-Emitting Diodes. *Adv. Mater.* **2021**, *33*, 2100677.
(8) Hartono, N. T. P.; Thapa, J.; Tiihonen, A.; Oviedo, F.; Batali, C.; Yoo, J. J.; Liu, Z.; Li, R.; Marrón, D. F.; Mougi, G.; Bawendi; Buonassisi, T.; Sun, S. How machine learning can help select capping layers to suppress perovskite degradation. *Nat. Commun.* **2020**, *11*, 4172.
(9) Li, Z.; Omidvar, N.; Chin, W. S.; Robb, E.; Morris, A.; Achenie, L.; Xin, H. Machine-Learning Energy Gaps of Porphyrins with Molecular Graph Representations. *J. Phys. Chem. A.* **2018**, *122*, 4571−4578.
(10) Momeni, K.; Ji, Y.; Wang, Y.; Paul, S.; Neshani, S.; Yilmaz, D. E.; Shin, Y. K.; Zhang, D.; Jiang, J.-W.; Park, H. S.; Sinnott, S.; van Duin, A.; Crespi, V.; Chen, L.-Q. Multiscale computational understanding and growth of 2D materials: a review. *npj Comput. Mater.* **2020**, *6*, 22.
(11) Weng, B.; Song, Z.; Zhu, R.; Yan, Q.; Sun, Q.; Grice, C. G.; Yan, Y.; Yin, W. J. Simple descriptor derived from symbolic regression accelerating the discovery of new perovskite catalysts. *Nat. Commun.* **2020**, *11*, 3513.
(12) Li, Y.; Lu, Y.; Huo, X.; Wei, D.; Meng, J.; Dong, J.; Qiao, B.; Zhao, S.; Xu, Z.; Song, D. Bandgap tuning strategy by cations and halide ions of lead halide perovskites learned from machine learning. *RSC Adv.* **2021**, *11*, 15688.
(13) Li, J.; Pradhan, B.; Gaur, S.; Thomas, J. Predictions and Strategies Learned from Machine Learning to Develop High-Performing Perovskite Solar Cells. *Adv. Energy Mater.* **2019**, *9*, 1901891.
(14) Majeed, N.; Saladina, M.; Krompiec, M.; Greedy, S.; Deibel, C.; MacKenzie, R. C. Using Deep Machine Learning to Understand the Physical Performance Bottlenecks in Novel Thin-Film Solar Cells. *Adv. Funct. Mater.* **2019**, *30*, 1907259.
(15) Sahu, H.; Rao, W.; Troisi, A.; Ma, H. Toward Predicting Efficiency of Organic Solar Cells via Machine Learning and Improved Descriptors. *Adv. Energy Mater.* **2018**, *8*, 1801032.
(16) Zhu, C.; Liu, W.; Li, Y.; Huo, X.; Li, H.; Guo, K.; Qiao, B.; Zhao, S.; Xu, Z.; Zhao, H.; Song, D. Key factors governing the device performance of CIGS solar cells: Insights from machine learning. *Sol. Energy* **2021**, *228*, 45.
(17) Janai, M. A. B.; Woon, K. L.; Chan, C. S. Design of efficient blue phosphorescent bottom emitting light emitting diodes by machine learning approach. *Org. Electron.* **2018**, *63*, 257.
(18) Ahn, D. H.; Lee, H.; Kim, S. W.; Karthik, D.; Lee, J.; Jeong, H.; Lee, J. Y.; Kwon, J. H. Highly Twisted Donor-Acceptor Boron Emitter and High Triplet Host Material for Highly Efficient Blue Thermally Activated Delayed Fluorescent Device. *ACS Appl. Mater. Interfaces* **2019**, *11*, 14909.
(19) Wang, S.; Kempen, D. H.; Simha, N. K.; Lewis, J. L.; Windebank, A. J.; Yaszemski, M. J.; Lu, L. Photo-Cross-Linked Hybrid Polymer Networks Consisting of Poly(propylene fumarate) and Poly(caprolactone fumarate): Controlled Physical Properties and Regulated Bone and Nerve Cell Responses. *Biomacromolecules* **2008**, *9*, 1229.
(20) Li, J.; Ding, D.; Tao, Y.; Wei, Y.; Chen, R.; Xie, L.; Huang, W.; Xu, H. A Significantly Twisted Spirocyclic Phosphine Oxide as a Universal Host for High-Efficiency Full-Color Thermally Activated Delayed Fluorescence Diodes. *Adv. Mater.* **2016**, *28*, 3122.
(21) Liang, X.; Tu, Z. L.; Zheng, Y. X. Thermally Activated Delayed Fluorescence Materials: Towards Realization o fHigh Efficiency through Strategic Small Molecular Design. *Chem. − Eur. J.* **2019**, *25*, 5623.
(22) Zeng, W.; Lai, H.-Y.; Lee, W.-K.; Jiao, M.; Shiu, Y.-J.; Zhong, C.; Gong, S.; Zhou, T.; Xie, G.; Sarma, M.; Wong, K.-T.; Wu, C.-C.; Yang, C. Achieving Nearly 30% External Quantum Efficiency for Orange−Red Organic Light Emitting Diodes by Employing Thermally Activated Delayed Fluorescence Emitters Composed of 1,8-Naphthalimide-Acridine Hybrids. *Adv. Mater.* **2017**, *30*, 1704961.

https://doi.org/10.1021/acsomega.1c06820
ACS Omega 2022, 7, 7893−7900